Petroleum Science 23 (2026) 1970–1985

Contents lists available at ScienceDirect

Petroleum Science

journal homepage: www.keaipublishing.com/en/journals/petroleum-science

Original Paper

Quantitative prediction of steam channeling based on steam override in horizontal wells cyclic steam stimulation: Mathematical modeling and experimental validation

Xiang-Xing Yan [a], Zhan-Xi Pang [a,*], Ling-Feng Fu [a], Chun-Hua Qin [a], Xiao-Hong Liu [b], Bo Wang [c]

[a] State Key Laboratory of Petroleum Resources and Engineering, China University of Petroleum (Beijing), Beijing, 102249, China
[b] Tianjin Branch of China National Offshore Oil Corporation (CNOOC) Ltd., Tianjin, 300452, China
[c] Henan Oilfield Institute, Sinopec China, Nanyang, 473400, Henan, China

ARTICLE INFO

Article history:
Received 14 September 2025
Received in revised form
28 October 2025
Accepted 19 December 2025
Available online 24 December 2025

Edited by Meng-Jiao Zhou

Keywords:
Cyclic steam stimulation
Heavy oil
Steam channeling
Horizontal well
Mathematical model
Steam override
3D physical simulation experiment

ABSTRACT

Cyclic steam stimulation (CSS) is a common method for heavy oil reservoir, but the current research on steam channeling in horizontal wells is limited. This study proposes a novel mathematical model based on steam override to predict steam channeling during the CSS process in horizontal wells, focusing on the quantization of the heated region, steam front edge position, and steam channeling time. The model was validated through a 3D physical simulation experiment. The experimental results were broadly consistent with the theoretical predictions. The study finds that steam channel is an upward-curved wedge shape, making it difficult to mobilize the bottom reservoir. The steam channeling time was predicted to be 10.10 min, with an 11.16% error compared to the experimental value of 8.97 min. Furthermore, the introduction of foam increased the oil steam ratio from 1.52 to 1.92. Reducing appropriately the steam injection rate, increasing well spacing, and decreasing steam temperature, together with periodic foam injection, can delay steam channeling. In conclusion, the model offers practical insights for steam channel prediction, which can improve the effectiveness of steam injection strategies in heavy oil reservoirs.

1. Introduction

The reserves of heavy oil in the world are abundant with a wide distribution range (Sasaki et al., 1996; Hein, 2017; Sun et al., 2017). Thermal recovery techniques have long been the cornerstone of heavy oil exploitation, since its first application in 1966 (Khan and Parag, 1992; Ahmadi, 2023). Particularly in high viscosity and low fluidity oil reservoirs, steam is usually chosen as the heat medium (Giacchetta et al., 2015; Chen et al., 2018; Dong et al., 2019). These thermal recovery techniques, including cyclic steam stimulation (CSS), steam flooding (SF) and steam-assisted gravity drainage (SAGD), have demonstrated significant potential in enhancing oil recovery by reducing oil viscosity and improving oil flow capacity (Shi et al., 2019; Liu et al., 2020; Dong et al., 2022; Sandoval et al., 2023). Owing to its strong applicability, high efficiency, and simple operation, CSS has become the primary development method for most heavy oil fields in global scale (Tagavifar et al., 2016; Zhang et al., 2021). CSS as the first step of thermal recovery, usually lasts for multiple cycles. Typically, in each cycle, steam injection and well soaking are carried out first, followed by the production of heated oil (Bao et al., 2016; Pawelec et al., 2016; Wu et al., 2018). While extensive studies have focused on vertical wells, the unique challenges posed by horizontal well configurations, especially in steam channeling of CSS operations, remain inadequately addressed (Huang et al., 2018a, 2018b).

Based on the principle of energy conservation, an analytical mathematical model for predicting the evolution of heated region during the injection stage of vertical wells CSS was proposed by Marx and Langenheim (1959). This is the earliest CSS thermal recovery mathematical model, which provides a lot of assistance for

* Corresponding author.
E-mail address: pxiad9827@cup.edu.cn (Z.-X. Pang).
Peer review under the responsibility of China University of Petroleum (Beijing).

https://doi.org/10.1016/j.petsci.2025.12.032

later research. Boberg and Lantz developed the first analytical model for CSS in vertical wells based on Langenheim's model (Boberg and Lantz, 1966), the model provided considerable assistance for on-site guidance. Based on the principle of diversion, Lookeren conducted a study on the changes in the steam chamber of radial flow in horizontal strata (Lookeren, 1983). A steam chamber distribution model considering steam override for CSS in vertical wells was proposed. By considering the potential gradient of steam and oil at each point on the steam-liquid interface with respect to the radius, meanwhile, introducing the pseudo-flow ratio, a calculation formula for the front edge of steam displacement was obtained. It was widely applied in the vertical wells CSS at that time, but this model still could not be used in the field of horizontal wells. Afterwards, numerical simulation technology was combined with CSS technology for the exploitation of heavy oil resources (Settari and Raisbeck, 1981; Boberg et al., 1992) and achieved good results in the oilfield of Sudan (Tewari et al., 2011). With the reduced costs of drilling and technology progress, compared with vertical wells, horizontal well has technical advantages such as expanding heated region, facilitating lateral transportation of fluids and enhancing thermal efficiency (Zhu et al., 2017; Escobar et al., 2000). Therefore, the application of horizontal wells CSS technology in heavy oil reservoirs has emerged as a more prevalent situation (Wang et al., 2023; Satar and Ozturk, 2024). It has also led to an increasing number of production problems of horizontal wells that need to be solved. In horizontal wells CSS process, both of the evolution tendency of heated region and the accurate calculation of production performance are significant (Gontijo and Aziz, 1984; Sylvester and Chen, 1988; Tamim and Ali, 1998; Miah et al., 2018; He et al., 2019). Research in this area can not only explore the difficulties and keys of CSS production in horizontal wells in complex reservoirs, but also provide strong support for on-site production. Wu et al. proposed a semi-analytical model in shallowly buried thin layer of heavy oil (Wu et al., 2009). In this model, the steam override phenomenon, reservoir heat loss and the mechanisms of two-phase flow were taken into consideration, but it was still not applicable in thick layers of heavy oil reservoirs. Saripalli et al. established a new semi-analytical model for predicting oil production (Saripalli et al., 2018). The situation where reservoir thickness significantly exceeded the expansion of heated region was considered, a method for calculating the temperature within it was proposed. All the above-mentioned models adhered to the isothermal assumption in different heated regions and none of them considered the heat impact caused by the phase change of steam.

In the realm of horizontal wells steam stimulation, steam channeling exhibits a complex three-dimensional steam migration pattern (Okoye and Tiab, 1982; Tiab et al., 1982). Due to the combined effects of steam override, permeability anisotropy and thermal stress redistribution, the structure of steam channel has become increasingly complex, this situation was regarded as a pervasive yet poorly quantified phenomenon (Pratama and Babadagli, 2020; Li et al., 2020; Pang et al., 2021). Previous studies have primarily relied on simplified 2D models to characterize steam channeling in vertical wells, due to the lack of consideration in the vertical direction of the reservoir, the spatial heterogeneity of horizontal well environments was neglected (Li et al., 2023; Zhang et al., 2023a). Therefore, these models cannot be directly applied to the CSS production of horizontal wells. Furthermore, the evolution of steam channel during CSS remains unclear, which leads to the difficulty in later strategies such as nitrogen foam, viscosity reducer, high-temperature gel, and thermal solidification agent (Sharifipour et al., 2019; Tao et al., 2022; Zhang et al., 2023b; Pang et al., 2024). In summary, previous studies have not established a mathematical model for steam channeling in horizontal wells CSS, and relevant experiments are scarce (Li et al., 2022; Benyamin, 2023; Liu et al., 2023; Wang et al., 2024; Lin et al., 2025). The research of this article is expected to fill the gap in this field.

In this paper, based on the conservation of mass and energy, a mathematical model for steam channeling of horizontal wells CSS, which considered steam override and heterogeneity was established. Compared with the previous models that only considered a single situation of oil reservoir, the new model established in this paper has a higher similarity to the actual oil reservoir and can be widely applied to the prediction of steam channeling in the horizontal wells CCS. Not only the position of the steam front edge and the steam channeling time can be determined, but also the volumes of the steam chamber and the condensed water zone can be quantitatively calculated. Furthermore, to verify this mathematical model, based on the principle of similarity criterion, a 3D physical simulation experiment of horizontal wells CSS was designed and carried out. The calculation results of the mathematical model were highly consistent with the experimental results, verifying the correctness of the mathematical model. Then, the influencing parameters of the steam channel interface were analyzed. Based on the parameters of a certain oil field, position of the steam front edge, steam channeling time, volume of the steam chamber and volume of the condensed water zone were calculated actually. This achievement demonstrates strong engineering application potential.

2. Mathematical model

Steam channeling models for vertical wells have been investigated, whereas steam channeling in horizontal well systems has received comparatively limited attention. Steam injection in horizontal wells initially propagates in a radial flow pattern from the wellbore to the reservoir. However, due to the steam override, steam channels present a curved wedge-shaped structure, as shown in Fig. 1(a). By analyzing representative reservoir cross-sections, the areas of the steam chamber and condensed water zone can be quantified, and the front position of steam chamber and steam channeling time in horizontal wells can be calculated.

2.1. Steam channeling model

A steam channeling cross-section is taken from the reservoir model. The steam channeling model of horizontal wells can be simplified as shown in Fig. 1(b). In the heated region between two wells, there are steam chamber, transition interface, and condensed water zone. Furthermore, the model of steam channeling cross-section is differentiated and divided into n equal parts along the flow direction, simplifying it into two right-angle trapezoids as shown in Fig. 1(c). The following assumptions are made for this model: (1) The cold oil zone outside the heated region has no flow characteristics; (2) The thermal properties of the cold oil zone, top and bottom layers where the horizontal well is located, do not change with the variation in formation temperature during steam injection; (3) The front edge of the condensed water to the production well is considered as steam channeling, and the temperature at the front edge of the steam chamber is the same as that at the rear end of the condensed water, with no heat conduction occurring (Lookeren, 1983). To ensure that the mathematical model had an analytical solution, the complex reservoir dynamics such as permeability heterogeneity, steam flow instability, and phase change effects in these assumptions were simplified. Based on the feedback from the oilfield, the calculation error was within an acceptable range.

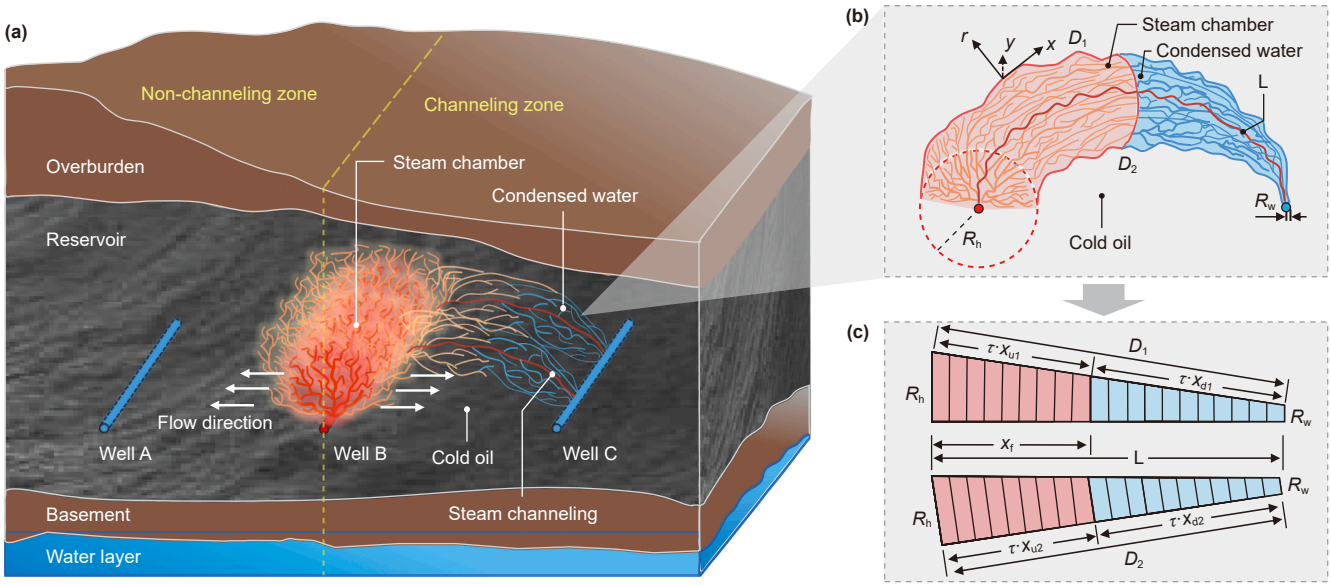

Fig. 1. Steam channeling model of horizonal wells. **(a)** Schematic of steam channels structure in reservoir; **(b)** schematic of steam channeling cross-section; **(c)** simplified form of steam channeling.

Two-dimensional heat conduction equation of energy conservation is established as follows:

$$\frac{\partial^2 T}{\partial r^2} = \frac{1}{\alpha_o}\frac{\partial T}{\partial t} \tag{1}$$

where T is the temperature, °C; r is the distance from a point to the middle steam channel, m; α_o is the thermal diffusivity coefficient, m^2/s; t is the time, d.

Initial conditions can be expressed as follows:

$$T(r,t)|_{r=0} = T_s, T(r,t)|_{t=0} = T_i \tag{2}$$

where T_s and T_i are the steam and initial reservoir temperature, respectively, °C.

Boundary condition can be expressed as follows:

$$T(r,t)|_{r\to\infty,t=0} = T_i \tag{3}$$

Based on Eqs. (1)–(3), the temperature at a certain point along the steam channel towards the cold oil zone can be expressed as:

$$T = T_s - (T_s - T_i)\frac{2}{\sqrt{\pi}}\int_0^{\frac{r}{2\sqrt{\alpha_o t}}} e^{-x^2}\,dx \tag{4}$$

The temperature gradient between the steam channel and the cold oil zone can be expressed as:

$$\frac{\partial T}{\partial r} = (T_s - T_i)\left(\frac{e^{-\frac{r^2}{4\alpha_o t}}}{\sqrt{\pi\alpha_o t}} - \frac{r^2 e^{-\frac{r^2}{4\alpha_o t}}}{2\alpha_o t\sqrt{\pi\alpha_o t}}\right) \tag{5}$$

The temperature gradient between the steam channel and the cold oil zone when $r = 0$ can be expressed as:

$$\left.\frac{\partial T}{\partial r}\right|_{r=0} = \frac{T_s - T_i}{\sqrt{\pi\alpha_o t}} \tag{6}$$

2.2. Steam channel lower interface

A theoretical model for three-phase flow is established as shown in Fig. 2. During steam channeling, the lower interface of the steam channel forms. The shape of this lower interface is divided into two stages: the rising stage and the falling stage. Steam drives oil in the rising stage, and oil drives water in the falling stage. It is assumed that the potential at each point perpendicular to the formation plane is the same.

The pressure at each point on the steam-oil interface at the lateral distances R_1 and R_2 from the injection well is converted to the "$Z = h$" plane (Lookeren, 1983).

$$\begin{cases} \Phi_{s1} = P_{s1} - \rho_s g h_{s1} \\ \Phi_{s2} = P_{s2} - \rho_s g h_{s2} \\ \Phi_{o1} = P_{o1} - \rho_o g h_{o1} \\ \Phi_{o2} = P_{o2} - \rho_o g h_{o2} \end{cases} \tag{7}$$

where Φ_{s1} and Φ_{s2} are the potential of the steam phase at points 1 and 2, respectively, Pa; Φ_{o1} and Φ_{o2} are the potential of the oil

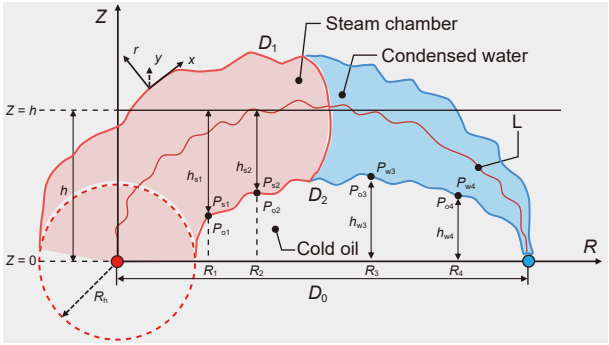

Fig. 2. The pressure and flow potential near the lower interface during the steam injection process.

phase at points 1 and 2, respectively, Pa; P_{s1} and P_{s2} are the pressure of the steam phase at points 1 and 2, respectively, Pa; P_{o1} and P_{o2} are the pressure of the oil phase at points 1 and 2, respectively, Pa; ρ_s and ρ_o are the density of steam and oil, respectively, kg/m^3; g is acceleration of gravity, m/s^2; h_{s1} and h_{s2} are the height of the steam phase at points 1 and 2, respectively, m; h_{o1} and h_{o2} are the height of the oil phase at points 1 and 2, respectively, m.

Therefore, the following equation holds:

$$\Delta\Phi_s - \Delta\Phi_o = (\rho_o - \rho_s)g\Delta h_s \tag{8}$$

where $\Delta\Phi_s$ is the potential difference of the steam phase between points 1 and 2, Pa; $\Delta\Phi_o$ is the potential difference of the oil phase between points 1 and 2, Pa; Δh_s is the height change during the rising stage of lower interface in steam channel, m.

By taking the partial derivative of Eq. (8) with respect to R, the shape of the rising stage in lower interface can be obtained:

$$\frac{\Delta h_s}{\partial R} = \frac{1}{(\rho_o - \rho_s)g}\left(\frac{\partial\Phi_s}{\partial R} - \frac{\partial\Phi_o}{\partial R}\right) \tag{9}$$

where R is the horizontal distance to the steam injection well, m.

Assuming stable two-phase flow of steam and oil, according to Darcy's law, the following equation is obtained:

$$\begin{cases} \dfrac{\partial\Phi_s}{\partial R} = -\dfrac{\mu_s i_s}{h_s\Delta y K_s\rho_s} \\ \dfrac{\partial\Phi_o}{\partial R} = -\dfrac{\mu_o i_o}{(h-h_s)\Delta y K_o\rho_o} \end{cases} \tag{10}$$

where μ_s and μ_o are the steam and oil viscosity, respectively, mPa·s; i_s and i_o are the mass flow rate of the steam and oil phase, respectively, t/d; h_s is the height of the rising stage on the steam channel lower interface, m; Δy is the thickness of high permeability zone along the horizontal well direction, m; K_s and K_o are the relative permeability of steam and oil phase, respectively, μm^2; h is the vertical distance to the steam injection well, m.

Substituting Eq. (10) into Eq. (9) gives:

$$\frac{\Delta h_s}{\partial R} = -\frac{\mu_s i_s}{h_s\Delta y K_s\rho_s(\rho_o-\rho_s)g}\left[1 - {M_1}^*\frac{h_s i_o i_s(R_b)}{(h-h_s)i_s i_o(R_e)}\right] \tag{11}$$

where M_1* is the pseudo mobility ratio between oil and steam, ${M_1}^* = \frac{\mu_o K_s}{\mu_s K_o}\cdot\frac{\rho_s i_o(R_e)}{\rho_o i_s(R_b)}$, dimensionless.

Because M_1* is much less than 1, Eq. (11) can be simplified, and after integration, the curve for the falling stage of lower interface is obtained:

$$h_s = \sqrt{\frac{2\mu_s i_s(R-R_h)}{\Delta y K_s\rho_s(\rho_o-\rho_s)g}} \tag{12}$$

where R_h is the radius of steam chamber, m.

Similarly, the pressure at each point on the oil-water interface at the lateral distances R_3 and R_4 from the injection well is converted to the "$Z = 0$" plane. The shape of the falling stage in lower interface is obtained:

$$\frac{\Delta h_w}{\partial R} = \frac{1}{(\rho_w-\rho_o)g}\left(\frac{\partial\Phi_o}{\partial R} - \frac{\partial\Phi_w}{\partial R}\right) \tag{13}$$

where Δh_w is the height change during the falling stage of lower interface in steam channel, m; ρ_w is the density of water, kg/m^3; Φ_w is the potential of the water phase, Pa.

Assuming stable two-phase flow of oil and water, according to Darcy's law, the following equation is obtained:

$$\begin{cases} \dfrac{\partial\Phi_o}{\partial R} = -\dfrac{\mu_o i_o}{h_w\Delta y K_o\rho_o} \\ \dfrac{\partial\Phi_w}{\partial R} = -\dfrac{\mu_w i_w}{(h-h_w)\Delta y K_w\rho_w} \end{cases} \tag{14}$$

where μ_w is the water viscosity, mPa·s; i_w is the mass flow rate of the water phase, t/d; h_w is the height of the falling stage on the steam channel lower interface, m; K_w is the relative permeability of water phase, μm^2.

Substituting Eq. (14) into Eq. (13) gives:

$$\frac{\Delta h_w}{\partial R} = -\frac{\mu_o i_o}{h_w\Delta y K_o\rho_o(\rho_w-\rho_o)g}\left[1 - {M_2}^*\frac{h_w i_w i_o(R_b)}{(h-h_s)i_o i_w(R_e)}\right] \tag{15}$$

where M_2* is the pseudo mobility ratio between water and oil, ${M_2}^* = \frac{\mu_w K_o}{\mu_o K_w}\cdot\frac{\rho_o i_w(R_e)}{\rho_w i_o(R_b)}$, dimensionless.

Because M_2* is much less than 1, Eq. (15) can be simplified, and after integration, the curve for the falling stage of lower interface is obtained:

$$h_w = \sqrt{\frac{2\mu_o i_o(D_0-R)}{\Delta y K_o\rho_o(\rho_w-\rho_o)g}} \tag{16}$$

where D_0 is the well spacing, m.

The following geometric relationship can be obtained:

$$\begin{cases} a\cdot(D_0 - R_h) = x_{u2} + x_{d2} \\ D_2 = \tau\cdot a\cdot(D_0 - R_h) \end{cases} \tag{17}$$

where a is the introduced ratio, dimensionless; x_{u2} and x_{d2} are the length of the rising and falling stage on the steam channel lower interface, respectively, m; D_2 is the length of the lower interface of steam channel, m; τ is the tortuosity factor, dimensionless.

Based on the geometric relationships shown in Fig. 1(c), the following relationship can be derived:

$$\begin{cases} (R_h - R_w)^2 + {D_2}^2 = L^2 \\ (R_h - R_w)^2 + L^2 = {D_1}^2 \\ \left(\dfrac{x_{u2}(R_h-R_w)}{x_{u2}+x_{d2}}\right)^2 + (\tau\cdot x_{u2})^2 = x_f^2 \\ \left(\dfrac{x_f(R_h-R_w)}{L}\right)^2 + x_f^2 = (\tau\cdot x_{u1})^2 \end{cases} \tag{18}$$

where R_w is the radius of well, m; L is the length of the middle steam channel, m; D_1 is the length of the higher interface of steam channel, m; x_f is the length of the steam front edge, m; x_{u1} is the length of the rising stage on the steam channel higher interface, m.

The areas of the steam chamber and the condensed water zone can be calculated as follows:

$$S_1 = R_h x_f\left(1 - \frac{x_f}{2L}\right)\left(1 + \frac{D_2}{L}\right) \tag{19}$$

$$S_2 = R_w(L + D_2)\left(1 - \frac{x_f}{L}\right) + \frac{R_h}{2}\left[\frac{\left(L - x_f\right)^2}{L}\left(1 + \frac{D_2}{L}\right)\right] \tag{20}$$

where S_1 and S_2 are the area of the steam chamber and condensed water zone, respectively, m^2.

2.3. Steam channeling time

According to the previous assumptions, there is no heat conduction at the interface between the steam chamber and condensed water. The reason for steam condensation is that heat transfers from the heated region to the cold oil zone. Therefore, based on the energy conservation principle, the latent heat of steam released at the interface between the thermal wave zone and cold oil zone equals the heat absorbed by the cold oil zone.

$$G_s(t)\rho_s L_v = \lambda_o \Delta y \tau (x_{u1} + x_{u2}) \cdot \frac{(T_s - T_i)}{\sqrt{\pi \alpha_o t}} \tag{21}$$

where G_s is the instantaneous steam condensation volume, m^3/s; L_v is the latent heat of steam, kJ/kg; λ_o is the oil thermal conductivity, W/(m·K).

The mass conservation equation for the process of steam condensing into water can be expressed as:

$$\rho_w V_w = \rho_s V_s \tag{22}$$

where V_w and V_s are the water and steam volume, respectively, m^3.

By integrating Eq. (21) with respect to time, the steam volume in the steam chamber at the steam channeling time can be expressed as:

$$V_s = \frac{\rho_w V_w}{\rho_s} = \int_0^{t_{sc}} G_s(t)\mathrm{d}t = \frac{2\lambda_o \Delta y \tau (x_{u1} + x_{u2})(T_s - T_i)}{\rho_s L_v \sqrt{\pi \alpha_o}} \cdot \sqrt{t_{sc}} \tag{23}$$

where t_{sc} is the steam channeling time, d.

Based on Eqs. (22) and (23), the following can be obtained:

$$\rho_w V_{wc} = \rho_s \cdot \frac{2\lambda_o \Delta y \tau (x_{u1} + x_{u2})(T_s - T_i)}{\rho_s L_v \sqrt{\pi \alpha_o}} \cdot \sqrt{t_{sc}} \tag{24}$$

where V_{wc} is the condensed water volume, m^3.

According to the mass conservation equation, the total mass of injected steam is the sum of the condensed water and the remaining steam in the steam chamber, which is expressed as:

$$V_{si} = V_{wc}\frac{\rho_w}{\rho_s} + V_{sr} \tag{25}$$

where V_{si} is the steam injection volume, m^3; V_{sr} is the remaining steam volume in steam channel, m^3.

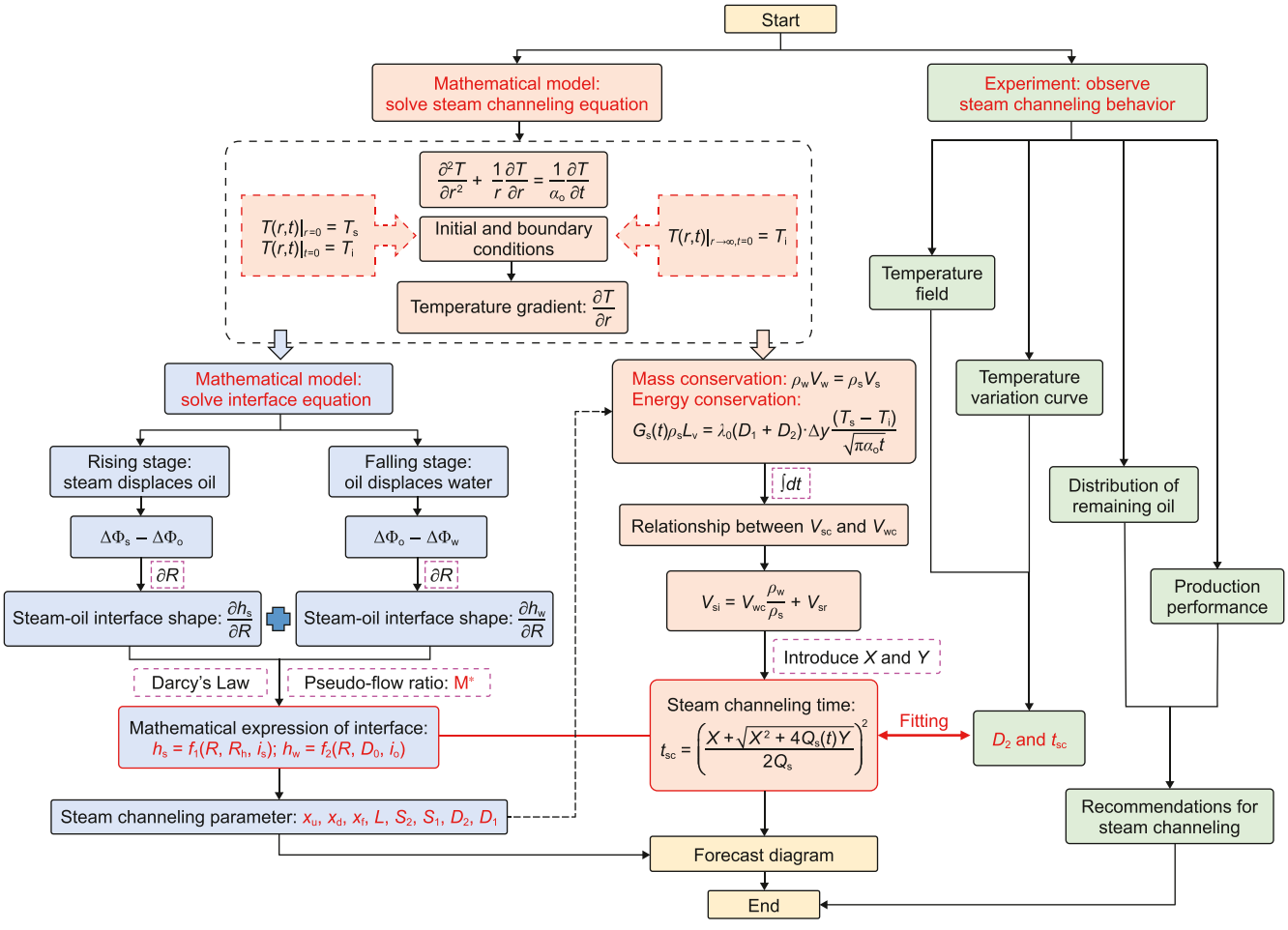

Fig. 3. Flowchart of steam channeling parameter calculation and validation.

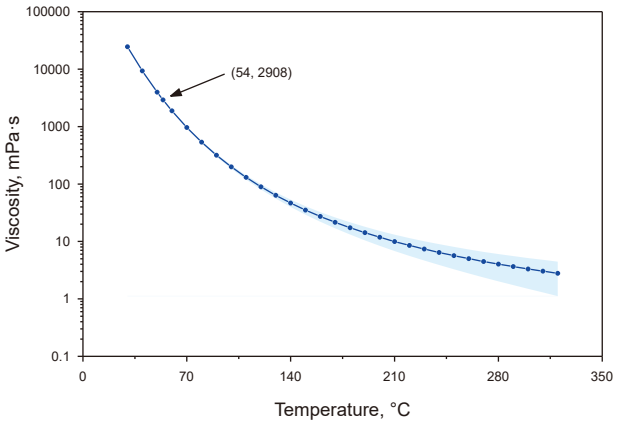

Fig. 4. Viscosity-temperature curve of the oil sample.

Table 1
Four key components percentages of the heavy oil sample.

Components	Colloid	Asphaltene	Wax	Sulfur
Percentages, %	28.6	6.48	1.24	0.43

Based on Eqs. (24) and (25), the following can be derived:

$$Q_s t_{sc} - \frac{2\lambda_o \Delta y \tau (x_{u1} + x_{u2})(T_s - T_i)}{\rho_s L_v \sqrt{\pi \alpha_o}} \cdot \sqrt{t_{sc}} - S_1 \cdot \Delta y \phi S_g = 0 \quad (26)$$

where Q_s is the steam injection rate, m^3/d; ϕ is the porosity, %; S_g is the gas saturation, %.

Let

$$\begin{cases} X = \dfrac{2\lambda_o \Delta y \tau (x_{u1} + x_{u2})(T_s - T_i)}{\rho_s L_v \sqrt{\pi \alpha_o}} \\ Y = S_1 \cdot \Delta y \phi S_g \end{cases} \quad (27)$$

where X and Y are the symbols introduced for calculation convenience, dimensionless.

Eq. (26) can be simplified as:

$$Q_s t_{sc} - X \cdot \sqrt{t_{sc}} - Y = 0 \quad (28)$$

By solving Eq. (28), the expression for the steam channeling time can be obtained:

$$t_{sc} = \left(\frac{X + \sqrt{X^2 + 4Q_s Y}}{2Q_s} \right)^2 \quad (29)$$

Based on the innovative approach, not only the front position of steam chamber and the steam channeling time can be determined, but the areas of the steam chamber and the condensed water zone can also be quantified. In order to validate this theoretical method, a 3D physical simulation experiment was designed based on similarity criteria to fit the theoretical parameters. The flowchart of the solution process is shown in Fig. 3.

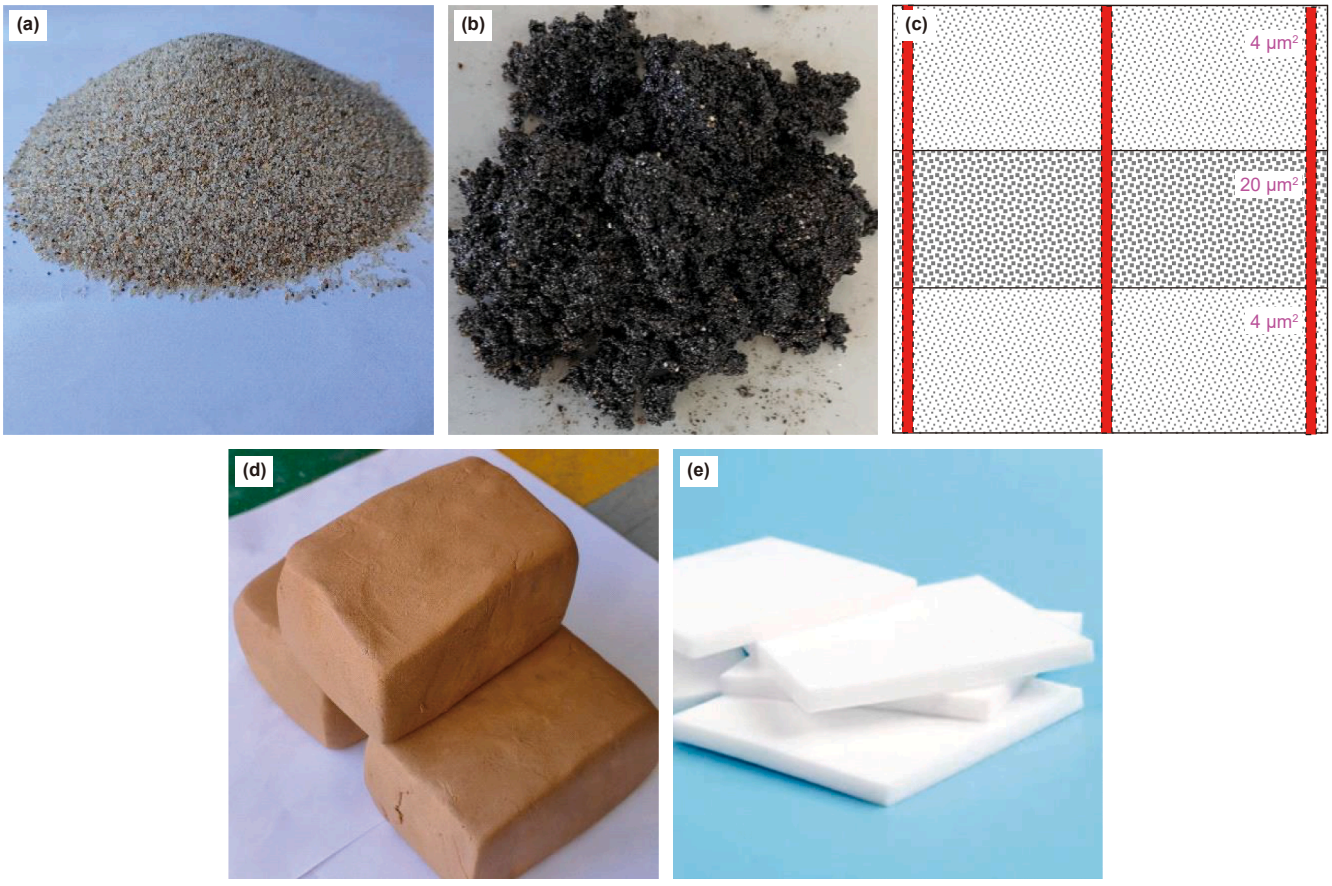

Fig. 5. Materials used in the experiment. **(a)** Quartz sand; **(b)** experimental oil sand; **(c)** oil sand filling method; **(d)** clay; **(e)** PTFE sheets.

3. Experiment

3.1. Experimental materials

The degassed crude oil was collected from a heavy oil field in China. Under atmospheric pressure, the oil sample has a density of 0.982 g/cm^3 at 20 °C and a viscosity of 2908 mPa·s at 54 °C. The viscosity-temperature curve of the oil sample is shown in Fig. 4. Table 1 presents four key components of the heavy oil sample: colloid, asphaltene, wax, and sulfur, along with their respective percentages. The formation water type is $CaCl_2$, with a salinity of 10,249.1 mg/L. Quartz sand (see Fig. 5(a)) was used to fill the experimental model, with particle sizes of 20–40 mesh and 40–60 mesh. The relationship between the quartz sand ratio and permeability was determined through multiple waterflood tests, and the experimental oil sand (see Fig. 5(b)) was prepared according to the determined ratio. In order to simulate steam channeling, a high-permeability zone was set in the middle of the reservoir (see Fig. 5(c)). Permeabilities of 4 μm^2 and 20 μm^2 correspond to low and high permeability reservoirs, respectively. Clay (see Fig. 5(d)) was used to fill the upper and lower layers of the experimental model. Polytetrafluoroethylene (PTFE) sheets (see Fig. 5(e)) were placed between the clay layer and the oil sand layer. Deionized water was heated by the steam generator to produce steam. The N_2 used in the experiment had a purity of 99.99%. The foaming agent used in the experiment was provided by the oilfield.

3.2. Experimental apparatus

The main experimental apparatus is shown in Fig. 6(a) and (b). They were composed of five main components: the injection

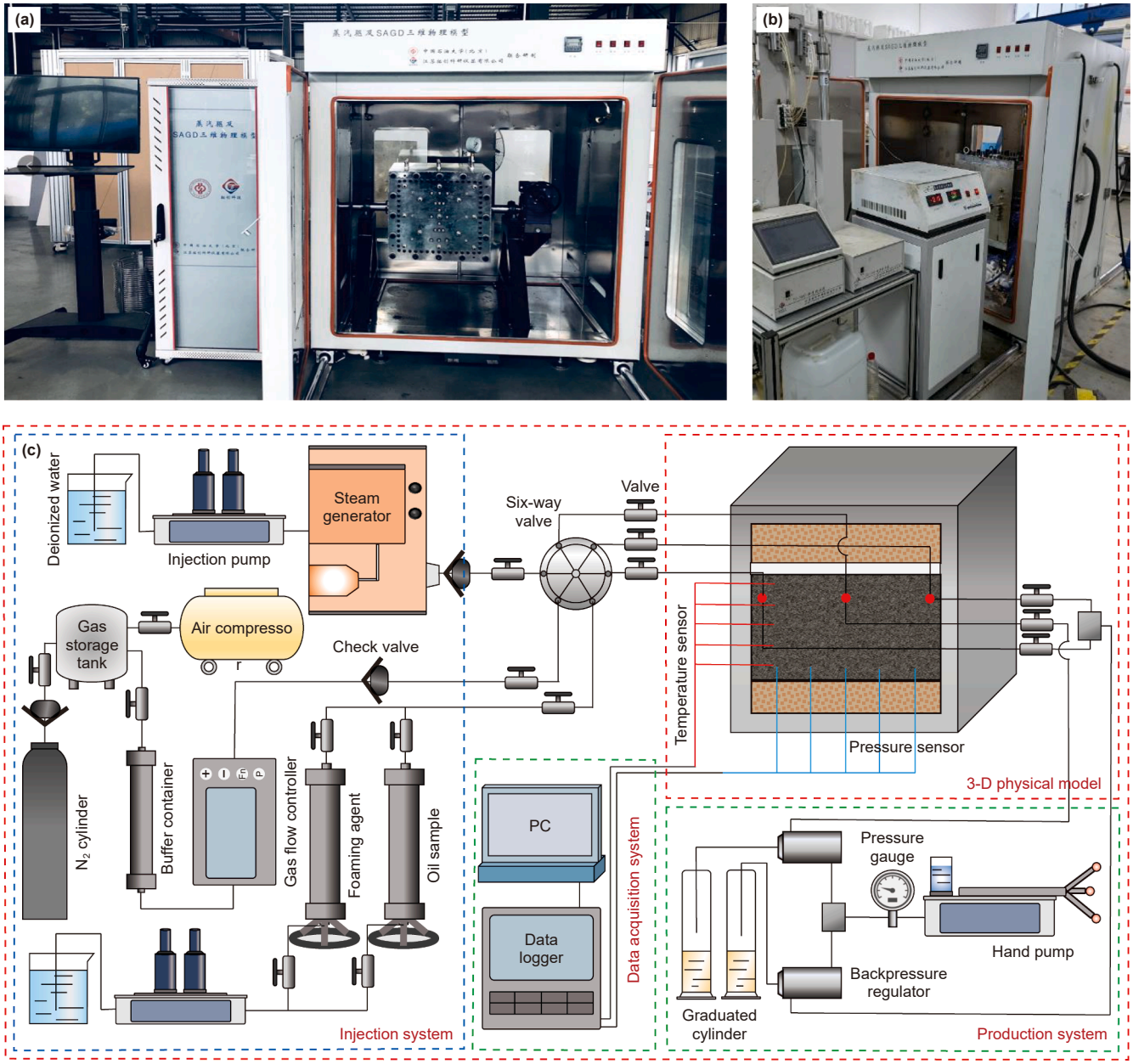

Fig. 6. Experimental apparatus and flowchart. **(a)** 3D physical model and data acquisition system; **(b)** injection system; **(c)** experimental flowchart.

system, the 3D physical model, the data acquisition system, the production system, and the auxiliary system. The experimental flowchart is shown in Fig. 6(c). The injection system included deionized water, N_2 cylinders, two dual-cylinder pumps, a steam generator, an air compressor, a gas storage tank, a buffer container, a gas flow controller, and two intermediate containers. The dual-cylinder pumps and gas flow controller could promptly monitor the fluid injection conditions. One of the intermediate containers contained oil sample, while the other contained a foaming agent solution with a concentration of 1 wt%. The 3D physical model (40 cm × 40 cm × 40 cm) was made of steel. The 3D model allowed simulation of oil layers with thicknesses ranging from 5 cm to 35 cm. It supported both horizontal and vertical well production modes. The data acquisition system was composed of a computer, a data logger, temperature and pressure sensors. This system had 208 temperature measurement points and 5 pressure measurement points, allowing real-time monitoring of temperature and pressure changes within the model. To ensure the accuracy of the experimental data, each thermocouple and pressure measurement point must be calibrated before the experiment begins. The production system included several graduated cylinders and a hand pump. The graduated cylinders were used to measure the produced liquid volume. The hand pump was used to provide back pressure. The auxiliary system included a constant temperature oven, a crane, a viscometer, an electronic balance, a thermal camera, electric heating tapes, and a series of valves. Before the experiment, the 3D model was heated to the initial reservoir temperature with the constant temperature oven. During the experiment, the oven reduced heat loss from the model, and the electric heating tapes were used to maintain the steam temperature and quality.

3.3. Experimental design

Based on the physical properties of the heavy oil reservoir, a 3D experiment for the CSS was designed. The oil and water samples were sourced from the oilfield. The porosity and oil saturation of the oil sand were consistent with those of the reservoir, and both the operating temperature and pressure were the same as those in the field. The thermal-physical properties of the quartz sand used in the 3D model were similar to those of the reservoir rock. Some parameters can be replicated in the 3D model, while others cannot be directly applied, such as the horizontal well length, reservoir thickness, steam injection volume per cycle, and soaking time. Therefore, it is necessary to convert field parameters into laboratory parameters with similarity criteria (Pang et al., 2019; Yan et al., 2025). The similarity criteria are shown in Table 2.

The similarity criteria are an effective experimental method in the laboratory (Pang et al., 2021). Before employing the similarity criteria, a scaling ratio $r(L)$ is required, typically denoted as:

$$r(L)=\frac{h_m}{h_p}=\frac{L_m}{L_p}=\frac{x_m}{x_p} \tag{30}$$

where $r(L)$ is the scaling ratio, dimensionless; h_m and h_p are the experimental and prototype reservoir thickness, respectively, m; L_m and L_p are the experimental and prototype well length, respectively, m; x_m and x_p are the experimental and prototype well spacing, respectively, m.

According to Eq. (30), experimental parameters can be calculated based on the values of oilfield parameters and similarity criteria. The detailed experimental parameters are provided in Table 3. It should be noted that the actual well length was 320 m, the experimental well length should ideally be 160 cm.

Table 2
Similarity criteria of CSS.

Similarity criterion	Physical significance	Simulation parameters
$\pi_1=\frac{K\rho_o gt}{\phi\Delta S\mu_o L}$	The ratio between gravity and viscous force	Permeability
$\pi_2=\frac{\lambda_r t}{\rho_r C_r L^2}$	The ratio between heat conductivity and heat capacity	Production time
$\pi_3=\frac{Kt}{\mu c\varphi L^2}$	Dimensionless elastic energy	Comprehensive compressibility
$\pi_4=\frac{i_s t}{\phi\Delta S\rho_w L^3}$	The mass ratio between steam injection and mobile oil	Steam injection flux
$\pi_5=\frac{\Delta P}{\rho_o gL}$	The ratio between pressure difference and gravity	Pressure difference

Table 3
Experimental parameter table.

Category	Parameters	Field	Experiment
Basic parameters	Well radius	0.1 m	0.3 cm
	Well length	320 m	40 cm (1/4)
	Reservoir thickness	32 m	16 cm
	Porosity	30.1%	30.1%
	Initial oil saturation	65%	65%
	Permeability	1.87 μm^2	4 μm^2 20 μm^2
	Oil viscosity (54 °C)	2908 mPa·s	2908 mPa·s
	Initial temperature	54 °C	54 °C
	Steam quality	0.4	0.4
	Steam temperature	300 °C	300 °C
	Initial pressure	12 MPa	12 MPa
Injection parameters	Steam injection volume per cycle	1500 m^3 (1/4)	188 cm^3
	Injection time	20 d	15 min
	Soaking time	5 d	4 min
	Dosage of foaming agent per cycle	45 m^3	6 mL

However, due to limitations of the experimental model, only a length of 40 cm was used during experiments. This means that we only simulated one-fourth of the actual well length. Therefore, the steam injection volume should be correspondingly reduced.

The 3D model was filled based on the calculation results from the similarity criteria. The overall structure of the 3D model is shown in Fig. 7(a). The vertical distribution of the horizontal well and temperature sensors in the 3D experimental model is shown in Fig. 7(b). In addition, to simulate the reservoir heterogeneity and the steam channeling phenomenon, high-permeability and low-permeability zones were divided during the sand filling process, as shown in Fig. 7(c). It is worth noting that factors such as the sand filling method, varying compaction levels, uneven steam intake, substandard steam quality, and equipment malfunctions are potential sources of influence on the experiment.

3.4. Experimental procedure

The CSS experiment of horizonal wells was designed to simulate the formation process of steam channeling and explore the measures to control it. After steam channeling occurred, foam was applied to improve production performance. The temperature and pressure changes within the model were observed. The production performance and remaining oil distribution characteristics were analyzed. The experiment consists of three main stages: preparation stage, steam stage, and steam + foam stage.

Preparation stage: (1) Before conducting the horizontal well steam injection experiment, the quartz sand was cleaned and dried to prevent dust and impurities. (2) Sand packing tube experiments were carried out, and the quartz sand ratio was determined by the Darcy's law. (3) The prepared quartz sand, oil sample, and formation water were mixed to form experimental oil-sand (the oil saturation was 65%, and the water saturation was 35%). (4) Steel filter screens were used to wrap the simulated wellbore to prevent sand production. (5) The accuracy of temperature and pressure sensors was examined. (6) The oil-sand, clay, PTFE sheet, production wells, temperature and pressure sensors were placed according to the design at the fixed locations in the model. The model cover was sealed by graphite strips. (7) Before the experiment was carried out, N_2 was injected into the experimental model at 5 MPa, monitoring the pressure change within 24 h to ensure gas tightness of the experimental system. (8) The 3D model was heated to the initial reservoir temperature. (9) The oil and water sample were injected into the model at a low flow rate of 1 mL/min, until the pressure reached the experimental value. (10) The steam generator was turned on in advance to ensure steam quality.

Steam stage: Injection parameters calculated based on similarity criteria were used to conduct steam injection, soaking, and

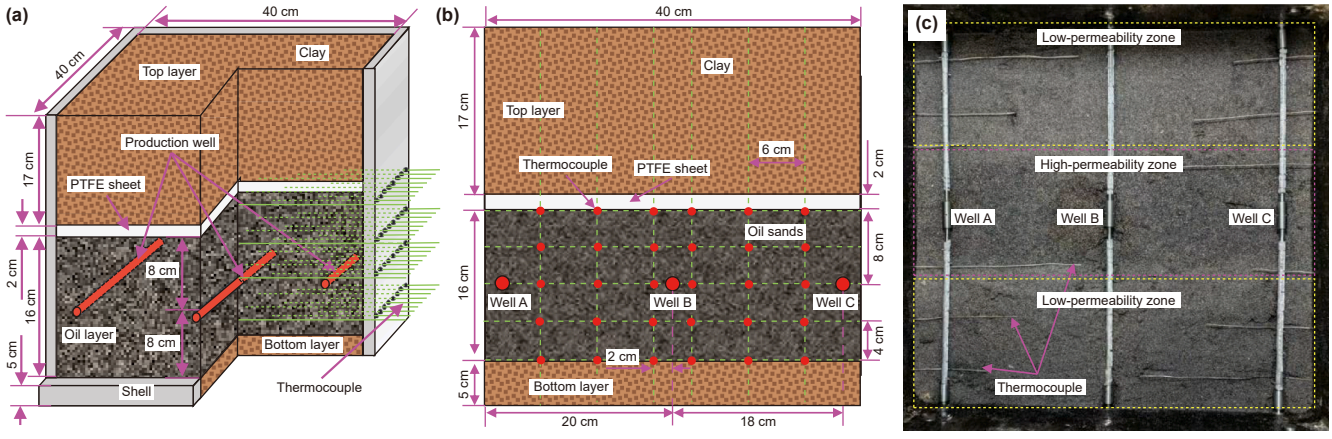

Fig. 7. Schematic of the 3D physical model. **(a)** Overall structure; **(b)** vertical distribution; **(c)** horizontal distribution.

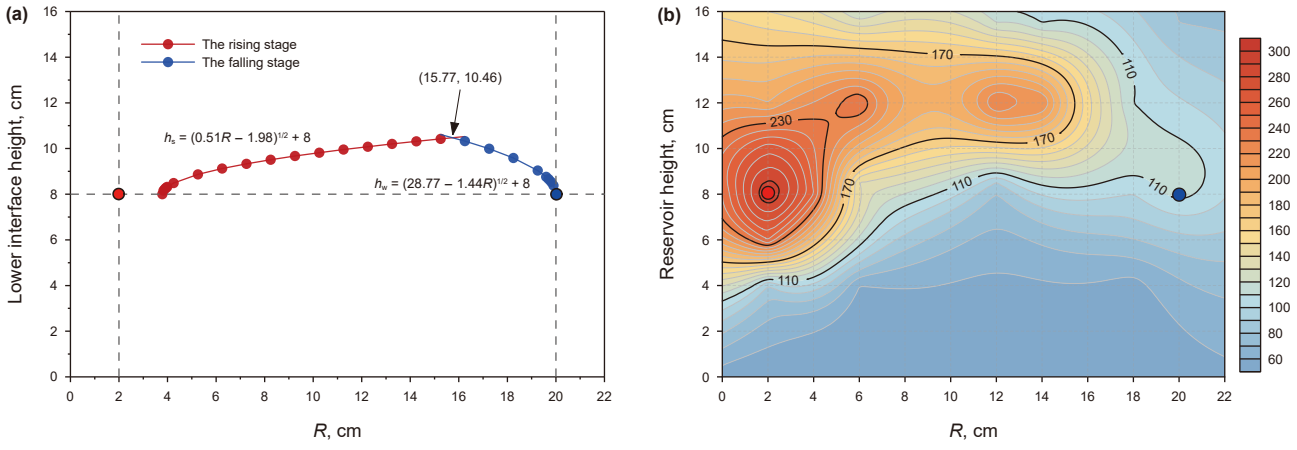

Fig. 8. The fitting result of the lower interface at steam channeling time. **(a)** The calculated shape of the lower interface; **(b)** vertical temperature field in experimental model.

oil production operations. Cyclic steam stimulation was performed in the order of well B – well C – well A. The steam injection volume was increased by 10% for each cycle. Production performance, temperature and pressure changes were recorded until the end of experiment.

Steam + foam stage: During steam injection, the temperature around the adjacent wells increased rapidly, indicating the occurrence of steam channeling. Foam was injected to block the steam channeling and maintain normal production. Temperature changes and production performance were continuously monitored to analyze the effectiveness of foam profiling.

4. Results and discussion

After the completion of the 3D physical simulation experiment, the calculated values from the mathematical model are fitted with the experimental results to assess the applicability of the mathematical model. Subsequently, the feasibility of the theoretical model in oilfield conditions is discussed.

4.1. Verification of D_2

In previous studies, the method of calculating the steam chamber radius based on the cyclic steam injection volume is

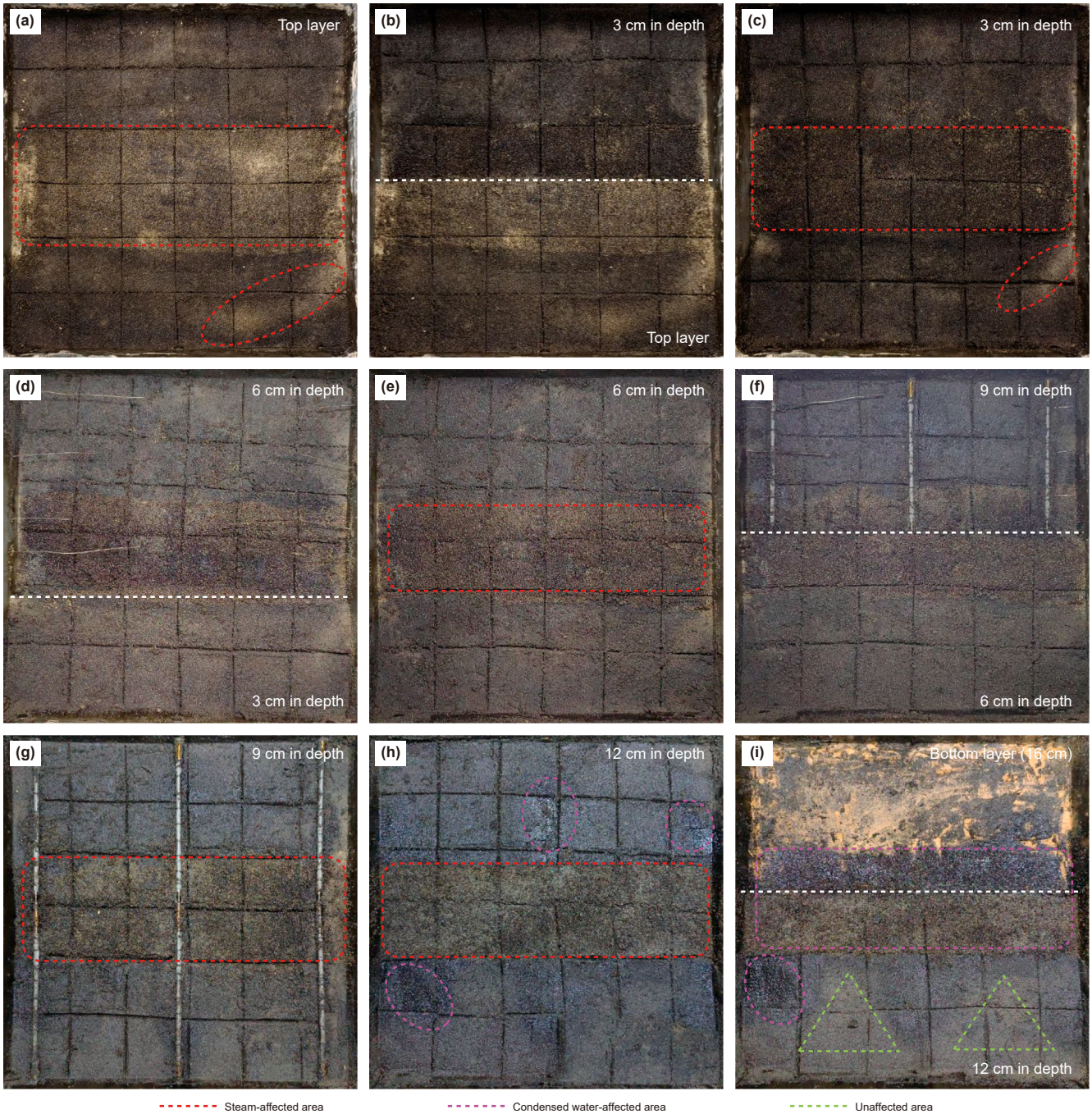

Fig. 9. Distribution of remaining oil in the experimental model. **(a)** The top layer; **(b)** comparison of the top layer and the 3 cm depth layer; **(c)** the 3 cm depth layer; **(d)** comparison of the 3 cm depth layer and 6 cm depth layer; **(e)** the 6 cm depth layer; **(f)** comparison of the 6 cm depth layer and 9 cm depth layer; **(g)** the 9 cm depth layer; **(h)** the 12 cm depth layer; **(i)** comparison of the 12 cm depth layer and 16 cm depth layer.

relatively mature (Ni and Cheng, 2005). For the target reservoir, the cyclic steam injection volume is 6000 t, the steam chamber radius is approximately 3.57 m. Converted to the 3D model, this corresponds to 1.79 cm. The predicted lower interface shape when steam override occurs is shown in Fig. 8(a). During the experiment, the vertical temperature field of the model when steam override occurs is shown in Fig. 8(b). It can be observed that the steam channel shape is similar to that assumed in Fig. 1(b), which confirms the appropriateness of the assumption. The lower interface shape obtained from the calculations shows a good fit with the results from the experiment, indicating that the theoretical model can adequately fit the lower interface shape of the heating range.

Fig. 9(a)–(i) show the distribution of remaining oil after the CSS experimental. The red line marks the steam-affected area, the pink line marks the condensed water-affected area, and the green line marks the unaffected area. It can be observed that, due to the effects of steam override and steam channeling, the high-permeability zone and parts of low-permeability zone in the upper layer have a low oil saturation. In the upper part of the production well, the oil sand is generally mobilized. The trajectory of low saturation zone is generally consistent with the theoretical trajectory shown in Fig. 8(a), indicating that the mathematical model provides accurate calculations. As the sampling depth increases, the oil saturation in the oil sand gradually increases, and the steam invasion area decreases. In the lower part of the production well, the majority of the oil sand is affected by condensed water, with a low recovery degree, and some unaffected areas are even present.

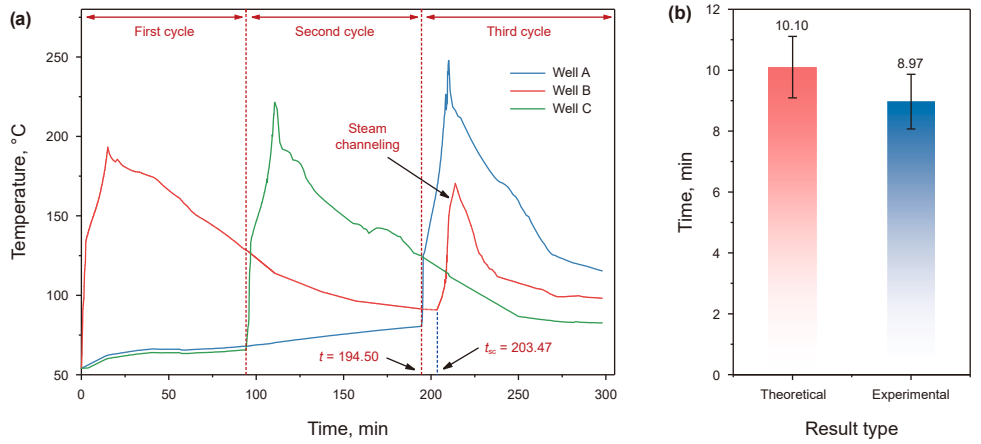

Fig. 10. The fitting result of the steam channeling time. **(a)** Temperature variation curve around the production well in experimental model; **(b)** comparison of steam channeling time.

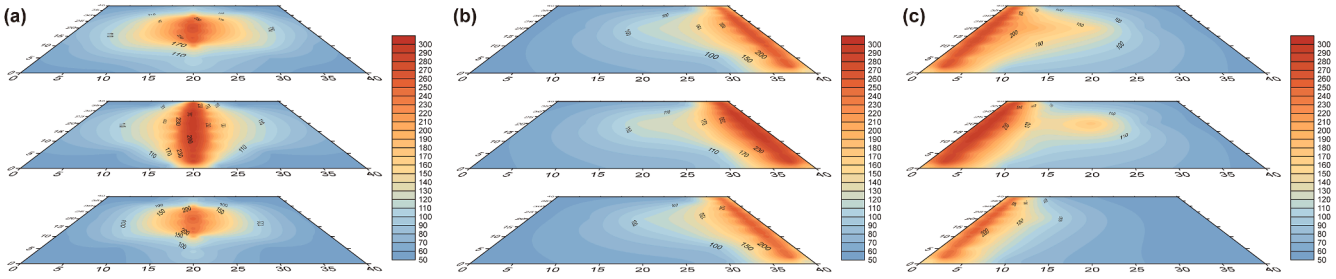

Fig. 11. Temperature fields in experimental model. **(a)** First cycle; **(b)** second cycle; **(c)** third cycle.

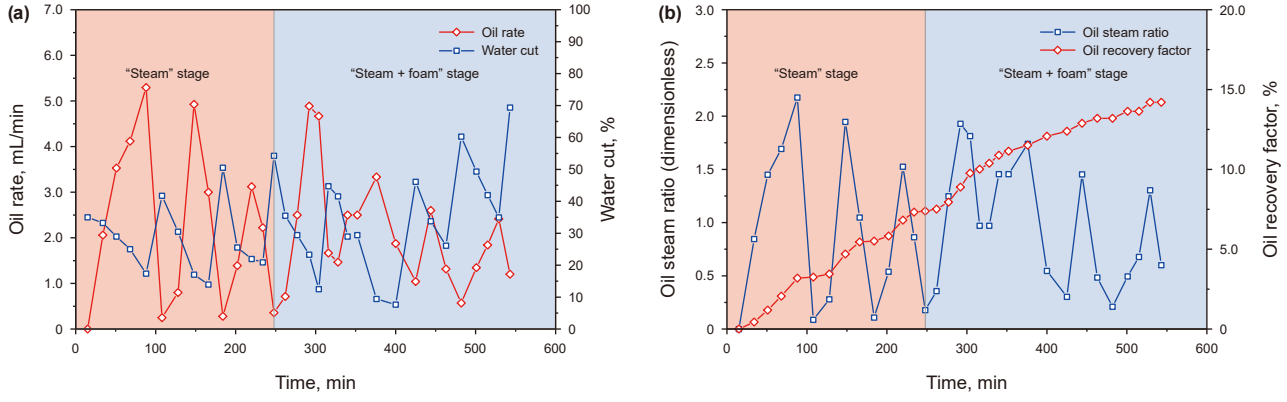

Fig. 12. The curves of production performance. **(a)** Oil rate and water cut; **(b)** oil steam ratio and oil recovery factor.

4.2. Verification of t_{sc}

Three thermocouples located near the three wells in the high-permeability zone are selected. By observing their temperature variations, the steam channeling process of horizontal well CSS is analyzed. Fig. 10(a) presents the temperature changes in the near-well zone during the steam phase. It can be observed that, during the third cycle of CSS, steam is injected in Well A at 194.50 min. At 203.47 min, steam starts to channel from Well A to Well B, and the temperature in the near-well zone of Well B rises rapidly. Steam injection stops at 210.17 min, the temperature around Well B reaches 170.0 °C. Fig. 10(b) shows a comparison between the theoretical and experimental steam channeling time. The theoretical time is 10.1 min, while the experimental time is 8.97 min, with an error of 11.16%. This indicates that the theoretical model provides an accurate prediction. The actual steam channeling time is shorter than the theoretical time. The discrepancy may be caused by differences in compaction between wells A and B, which leads to an uneven permeability distribution and steam channeling early.

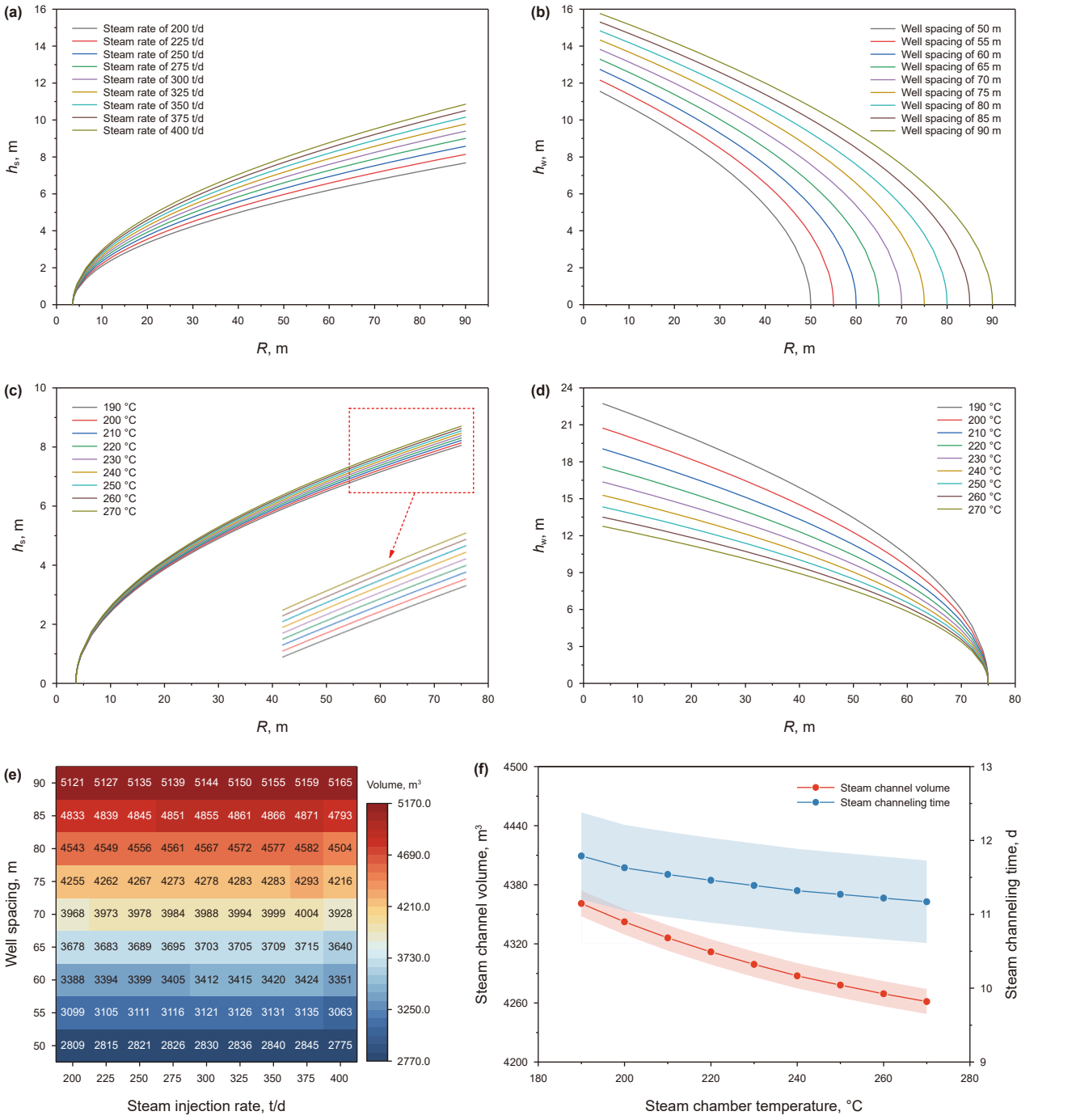

Fig. 13. Further study of the mathematical model. **(a)** h_s curves corresponding to different steam injection rates; **(b)** h_w curves corresponding to different well spacing; **(c)** h_s curves corresponding to different steam chamber temperatures; **(d)** h_w curves corresponding to different steam chamber temperatures; **(e)** heatmap of steam channel volume; **(f)** the effect of different steam chamber temperatures on steam channeling.

Table 4
Basic parameters of oilfield.

Parameters	Values
Injection steam mass per cycle, t	6000
Injection rate, t/d	300
Well spacing, m	75
Temperature of steam chamber, °C	250
Viscosity of steam, mPa·s	0.01745
Viscosity of oil, mPa·s	5.66
Thickness of high permeability zone, m	40
Density of oil, kg/m^3	776.80
Density of steam, kg/m^3	19.98
Density of water, kg/m^3	799.23
Gravitational acceleration, m/s^2	9.80
Tortuosity, dimensionless	1.30 (Pang et al., 2018)

The temperature fields of three cycles after steam injection are shown in Fig. 11(a)–(c). It can be observed that after steam injection in each cycle, steam is mainly distributed around the horizontal well and in the high permeability zone. After the completion of steam injection in the Well B, the steam chamber takes on a diamond shape, while after the steam injection in the two edge wells, the steam chamber takes on a triangular shape. At the end of the third cycle of steam injection, the temperature field clearly demonstrates steam flow from Well A to B, and the steam channel presents a curved wedge-shaped structure. This confirms the validity of the shape assumption in the mathematical model.

Fig. 12(a), (b) present the relationship curves between time and oil rate, water cut, oil steam ratio, and oil recovery factor. It can be observed that during the steam stage, the peak oil rate initially rises to 5.29 mL/min and then drops to 3.12 mL/min in the third cycle. The water cut increases from 35% to 54.26%, and the peak oil steam ratio reaches 2.17. After the occurrence of steam channeling, the peak oil steam ratio decays to 1.52, and the oil recovery factor for this stage is 7.39%. After the introduction of foam, the peak oil rate in the fourth cycle reaches 4.89 mL/min, returning to the pre-steam channeling level. The oil rate in the fifth cycle is slightly higher than that after steam channeling, but in the subsequent sixth and seventh cycles, the oil rate continuously decreases, indicating that the profile control effect of foam gradually deteriorates. The water cut shows a trend of decreasing and then increasing, and reaches 69.35% at the end of the seventh cycle. The peak oil steam ratio during this stage rises to 1.92, and the oil recovery factor reaches 14.20%. Because of the foam profile control, steam thermal efficiency is improved, providing a guarantee for sustained oil production. However, it is evident that the effectiveness of foam gradually decreases.

4.3. Discussion

After confirming the effectiveness of the mathematical model, the trajectories of the rising and falling stages of the steam channel lower interface are analyzed. If the cyclic steam injection volume is 6000 t. Fig. 13(a), (c) show the h_s curves corresponding to different steam injection rates and steam chamber temperatures. It can be observed that the steam injection rate directly affects the shape of the h_s curve. The higher the steam injection rate, the faster the fluid flow velocity, and the higher the rise of the interface. Therefore, reducing the steam injection rate appropriately can mitigate steam override and steam channeling. The steam chamber temperature determines the steam density, and steam density directly affects the shape of the h_s curve. The higher the steam chamber temperature, the lower the steam density, and the higher the rise of the interface. Thus, decreasing the steam injection temperature appropriately can inhibit steam override.

Fig. 13(b), (d) show the h_w curves corresponding to different well spacing and steam chamber temperatures. It can be observed that the well spacing doesn't alter the shape of the h_w curve but directly determines the length of the falling trajectory. The larger the well spacing, the longer the trajectory of condensed water fall. Therefore, appropriately increasing the well spacing can delay the steam channeling. The steam chamber temperature determines the oil viscosity, and oil viscosity influences the shape of the h_w curve. The higher the steam chamber temperature, the lower the oil viscosity, and the lower the fall of the interface. Therefore, decreasing the steam temperature appropriately can delay the steam channeling.

Fig. 13(e) presents the heat map of the steam channel volume. From the heat map analysis, it can be observed that as the well

Table 5
Calculation results of related parameters.

Parameters	Values
Radius of steam chamber, m	3.57
Length of the rising stage, m	69.8057
Length of the falling stage, m	26.9801
Length of the lower interface, m	96.7858
Length of the main channel, m	96.8480
Length of the higher interface, m	96.9101
Length of the steam front edge, m	69.8506
Volume of the steam chamber, m^3	3898.72
Volume of the condensed water zone, m^3	379.28
Volume of the steam channel, m^3	4278.03
Steam channeling time, d	11.33

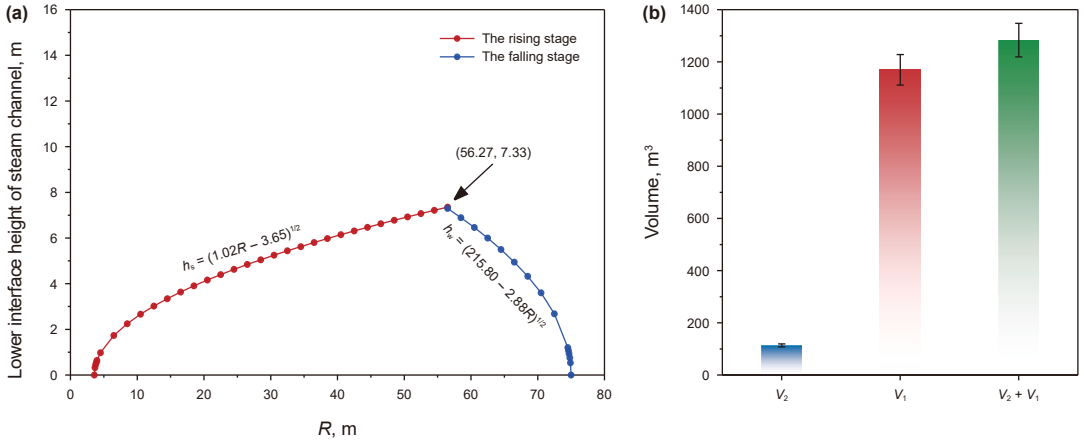

Fig. 14. Prediction results in the oilfield. **(a)** Shape of the lower interface of steam channel; **(b)** volume quantification of steam channel in different zones.

spacing increases, the volume of steam channel gradually increases. However, as the steam injection rate increases, the variation of the steam channel volume shows no obvious regularity. Therefore, it is recommended to optimize the combination of steam injection rate and well spacing to reduce unnecessary heat losses and improve overall production efficiency. Fig. 13(f) shows the corresponding steam channel volume and steam channeling time for different steam chamber temperatures. It can be observed that as the steam chamber temperature increases, the steam channel volume and the steam channeling time gradually decreases, indicating that high temperatures accelerate steam channeling without causing a larger steam channel volume.

Based on the theoretical and experimental results, several strategies can be proposed to control steam channeling. Appropriately reducing the steam injection rate and temperature can mitigate steam channeling by lowering the steam mobility and override. Increasing the well spacing within a reasonable range helps delay steam channeling by extending the falling trajectory of condensed water. In addition, the use of foam agents effectively improves steam sweep efficiency and oil recovery by enhancing profile control, but its effect weakens over multiple cycles. Therefore, optimizing the combination of steam injection rate, temperature, and well spacing, together with periodic foam injection, is recommended to improve steam utilization and maintain long-term production stability.

It is noteworthy that this mathematical method can be used to determine the position of the steam front edge, calculate the steam channeling time and quantify the steam channel for a specific reservoir. Given the basic parameters as shown in Table 4, with a steam injection rate of 300 t/d, a well spacing of 75 m, and a steam chamber temperature of 250 °C. The predicted lower interface shape of the steam channel is shown in Fig. 14(a). The intersection of the rising and falling stages occurs at (56.27, 7.33), indicating that when steam channeling occurs, the steam has migrated laterally for 56.27 m before condensing into water. At this point, the height of the lower interface of the steam channel is 7.33 m. Furthermore, the position of the steam front edge can be determined. The steam channel can be divided and quantified, the results are shown in Fig. 14(b). The total volume of the steam channel is 1283.41 m^3, and the volume of the steam chamber zone reaches 1169.62 m^3, accounting for 91.13%. The specific parameter calculation results are shown in Table 5.

5. Conclusions

In this study, based on the principles of mass and energy conservation, a novel model is designed to determine the position of steam front edge and calculate the steam channeling time, while achieving volume quantification of the steam channel. A 3D physical simulation experiment is designed based on similarity criteria. The accuracy of the mathematical model is validated by comparing theoretical and experimental results. Additionally, the proposed model is extended to parameters analysis and field applications. The main conclusions are as follows:

(1) The mathematical model accurately predicts the lower interface shape of steam channel. During the CSS process of horizontal wells, under the combined effect of the oil-steam density difference and the pressure differential, the steam channel forms an upward-curved wedge shape, making it difficult to mobilize the bottom reservoir.
(2) The mathematical model accurately predicts the steam channeling time. The experimental value of steam channeling time is 8.97 min, while the theoretical prediction time is 10.10 min, with a prediction error of 11.16%.
(3) In the steam stage, the peak oil steam ratio decreases from 2.17 to 1.52 because of steam channeling, and the oil recovery factor is 7.39%. After introducing foam, the peak oil steam ratio increases to 1.92, and the oil recovery factor is 14.20%.
(4) The rising stage of the steam channel is mainly influenced by steam injection rate and steam density, while the falling stage is affected by well spacing and oil viscosity. Optimizing the combination of steam rate, temperature, well spacing, and periodic foam injection, is recommended to delay steam channeling.
(5) For a specific reservoir condition, the steam front edge length is 69.85 m, the steam chamber volume is 3898.72 m^3, the condensed water zone volume is 379.28 m^3, and the steam breakthrough time is 11.33 d.

It should be noted that the study results are based on assumptions within the CSS process of horizontal wells. Future research can consider other dynamic parameters to further refine the prediction of steam channeling. These advancements will significantly enhance the prediction and control technologies for steam channeling.

CRediT authorship contribution statement

Xiang-Xing Yan: Writing – original draft, Validation, Investigation, Conceptualization. **Zhan-Xi Pang:** Supervision, Funding acquisition, Conceptualization. **Ling-Feng Fu:** Investigation, Conceptualization. **Chun-Hua Qin:** Validation, Investigation. **Xiao-Hong Liu:** Validation, Supervision. **Bo Wang:** Validation.

Declaration of competing interest

The authors declare no conflict of interest.

Acknowledgements

The study was supported by National Natural Science Foundation of China (52574063) and National Natural Science Foundation of China (52074321).

Nomenclature

Abbreviations

3D	Three-dimensional
CSS	Cyclic steam stimulation
SF	Steam flooding
SAGD	Steam assisted gravity drainage
PTFE	Polytetrafluoroethylene

Parameters

α_o	Thermal diffusivity coefficient, m^2/s
$\Delta\Phi_o$	Potential difference of the oil phase between points 1 and 2, Pa
$\Delta\Phi_s$	Potential difference of the steam phase between points 1 and 2, Pa
Δh_s	Height change during the rising stage of lower interface in steam channel, m
Δh_w	Height change during the falling stage of lower interface in steam channel, m
Δy	Thickness of high permeability zone along the horizontal well direction, m
λ_o	Oil thermal conductivity, W/(m·K)
μ_o	Oil viscosity, mPa·s

μ_s	Steam viscosity, mPa·s
μ_w	Water viscosity, mPa·s
π	Pi, dimensionless
ρ_o	Density of oil, kg/m^3
ρ_s	Density of steam, kg/m^3
ρ_w	Density of water, kg/m^3
τ	Tortuosity factor, dimensionless
ϕ	Porosity, %
Φ_{o1}	Potential of the oil phase at point 1, Pa
Φ_{o2}	Potential of the oil phase at point 2, Pa
Φ_{s1}	Potential of the steam phase at point 1, Pa
Φ_{s2}	Potential of the steam phase at point 2, Pa
Φ_w	Potential of the water phase, Pa
a	Introduced ratio, dimensionless
D_0	Well spacing, m
D_1	Length of the higher interface of steam channel, m
D_2	Length of the lower interface of steam channel, m
e	Euler's number, dimensionless
g	Acceleration of gravity, m/s^2
G_s	Instantaneous steam condensation volume, m^3/s
h	Vertical distance to the steam injection well, m
h_m	Experimental reservoir thickness, m
h_p	Prototype reservoir thickness, m
h_s	Height of the rising stage on the steam channel lower interface, m
h_{o1}	Height of the oil phase at point 1, m
h_{o2}	Height of the oil phase at point 2, m
h_{s1}	Height of the steam phase at point 1, m
h_{s2}	Height of the steam phase at point 2, m
h_w	Height of the falling stage on the steam channel lower interface, m
i_o	Mass flow rate of the oil phase, t/d
i_s	Mass flow rate of the steam phase, t/d
i_w	Mass flow rate of the water phase, t/d
K_o	Relative permeability of oil phase, μm^2
K_s	Relative permeability of steam phase, μm^2
K_w	Relative permeability of water phase, μm^2
L	Length of the middle steam channel, m
L_m	Experimental well length, m
L_p	Prototype well length, m
L_v	Latent heat of steam, kJ/kg
M_1*	Pseudo mobility ratio between oil and steam, dimensionless
M_2*	Pseudo mobility ratio between water and oil, dimensionless
P_{o1}	Pressure of the oil phase at point 1, Pa
P_{o2}	Pressure of the oil phase at point 2, Pa
P_{s1}	Pressure of the steam phase at point 1, Pa
P_{s2}	Pressure of the steam phase at point 2, Pa
Q_s	Steam injection rate, m^3/d
r	Distance from a point to the middle steam channel, m
$r(L)$	Scaling ratio, dimensionless
R	Horizontal distance to the steam injection well, m
R_h	Radius of steam chamber, m
R_w	Radius of well, m
S_1	Area of the steam chamber, m^2
S_2	Area of the condensed water zone, m^2
S_g	Gas saturation, %
t	Time, d
t_{sc}	Steam channeling time, d
T	Temperature, °C
T_i	Initial reservoir temperature, °C
T_s	Steam temperature, °C
V_s	Steam chamber volume, m^3
V_{si}	Steam injection volume, m^3
V_{sr}	Remaining steam volume in steam channel, m^3
V_w	Water volume, m^3
V_{wc}	Condensed water volume, m^3
x_{d1}	Length of the falling stage on the steam channel higher interface, m
x_{d2}	Length of the falling stage on the steam channel lower interface, m
x_f	Length of the steam front edge, m
x_m	Experimental well spacing, m
x_p	Prototype well spacing, m
x_{u1}	Length of the rising stage on the steam channel higher interface, m
x_{u2}	Length of the rising stage on the steam channel lower interface, m
X	A symbol introduced for calculation convenience, dimensionless
Y	A symbol introduced for calculation convenience, dimensionless

References

Ahmadi, M., 2023. Chapter eleven – practical challenges in reservoir simulation of in-situ thermal heavy oil recovery. Sustainable In-Situ Heavy Oil and Bitumen Recovery, 399–487. https://doi.org/10.1016/B978-0-323-90848-1.00002-9.

Bao, Y., Wang, J.Y., Gates, I.D., 2016. On the physics of cyclic steam stimulation. Energy 115, 969–985. https://doi.org/10.1016/j.energy.2016.09.031.

Benyamin, Y.J., 2023. An improved coupled flow-geomechanical model for cyclic steam stimulation. Petrol. Explor. Dev. 50 (5), 1206–1214. https://doi.org/10.1016/S1876-3804(23)60459-8.

Boberg, T.C., Lantz, R.B., 1966. Calculation of the production rate of a thermally stimulated well. J. Petrol. Technol. 18 (12), 1613–1623. https://doi.org/10.2118/1578-PA.

Boberg, T.C., Rotter, M.B., Stark, S.D., 1992. History match of multiwell simulation models of the cyclic steam stimulation process at cold Lake. SPE Reserv. Eng. 7 (3), 321–328. https://doi.org/10.2118/20743-PA.

Chen, J.B., Lang, X.M., Wang, Y.H., et al., 2018. Comparative evaluation of different non-condensable gases on thermal behaviors, kinetics, high pressure properties, and product characteristics of heavy oil. Energy Convers. Manag. 162, 13–25. https://doi.org/10.1016/j.enconman.2018.02.029.

Dong, X.H., Jiang, X.C., Zheng, W., et al., 2022. Discussion on the sweep efficiency of hybrid steam–chemical process in heavy oil reservoirs: An experimental study. Pet. Sci. 19 (6), 2905–2921. https://doi.org/10.1016/j.petsci.2022.06.018.

Dong, X.H., Liu, H.Q., Chen, Z.X., et al., 2019. Enhanced oil recovery techniques for heavy oil and oilsands reservoirs after steam injection. Appl. Energy 239, 1190–1211. https://doi.org/10.1016/j.apenergy.2019.01.244.

Escobar, E., Valko, P., Lee, W.J., et al., 2000. Optimization methodology for cyclic steam injection with horizontal wells. In: SPE/CIM International Conference on Horizontal Well Technology. https://doi.org/10.2118/65525-MS.

Giacchetta, G., Leporini, M., Marchetti, B., 2015. Economic and environmental analysis of a steam assisted gravity drainage (SAGD) facility for oil recovery from Canadian oil sands. Appl. Energy 142, 1–9. https://doi.org/10.1016/j.apenergy.2014.12.057.

Gontijo, J.E., Aziz, K., 1984. A simple analytical model for simulating heavy oil recovery by cyclic steam in pressure-depleted reservoirs. In: SPE Annual Technical Conference and Exhibition. https://doi.org/10.2118/13037-MS.

He, C.G., Xu, A.Z., Fan, Z.F., et al., 2019. An integrated model for productivity prediction of cyclic steam stimulation with horizontal well. Energy Sci. Eng. 7 (3), 962–973. https://doi.org/10.1002/ese3.325.

Hein, F.J., 2017. Geology of bitumen and heavy oil: An overview. J. Pet. Sci. Eng. 154, 551–563. https://doi.org/10.1016/j.petrol.2016.11.025.

Huang, S.J., Cao, M., Cheng, L.S., 2018a. Experimental study on aquathermolysis of different viscosity heavy oil with superheated steam. Energy Fuels 32 (4), 4850–4858. https://doi.org/10.1021/acs.energyfuels.8b00181.

Huang, S.J., Xia, Y., Xiong, H., et al., 2018b. A three-dimensional approach to model steam chamber expansion and production performance of SAGD process. Int. J. Heat Mass Tran. 127, 29–38. https://doi.org/10.1016/j.ijheatmasstransfer.2018.06.136.

Khan, J., Parag, D., 1992. Twenty-five years of oil recovery by steam injection. SPE/DOE Enhanced Oil Recovery Symposium. https://doi.org/10.2118/24198-MS.

Li, S.Y., Han, R., Wang, P., et al., 2022. Experimental investigation of innovative superheated vapor extraction technique in heavy oil reservoirs: A two-dimensional visual analysis. Energy 238, 121882. https://doi.org/10.1016/j.energy.2021.121882.

Li, S.Y., Peng, D.L., Feng, S.B., et al., 2023. Dimethyl ether-steam assisted gravity drainage: Physical 2D heavy oil simulation. Fuel 342, 127821. https://doi.org/10.1016/j.fuel.2023.127821.

Li, Y., Dai, C.L., Wu, Y.N., et al., 2020. A new type of gelled foam plugging agent with resistance to temperature, salt and dilution. IOP Conf. Ser. Earth Environ. Sci. 565 (1), 012051. https://doi.org/10.1088/1755-1315/565/1/012051.
Lin, T., Song, H.Z., Gu, Q.L., et al., 2025. Case study: Multi-component thermal fluid technology to enhance production on thin-bedded heavy oil reservoir in Bohai Bay of China. Energy Rep. 13, 2245–2254. https://doi.org/10.1016/j.egyr.2025.01.071.
Liu, H., Wang, Y., Xiong, H., et al., 2020. Semianalytical analysis of chamber growth and energy efficiency of solvent-assisted steam-gravity drainage considering the effect of reservoir heterogeneity along the horizontal well. Energy Fuels 5, 5777–5787. https://doi.org/10.1021/acs.energyfuels.0c00536.
Liu, Y.L., Zhang, C., Li, S.Y., et al., 2023. Study of steam heat transfer enhanced by CO_2 and chemical agents: In heavy oil production. Pet. Sci. 20 (2), 1030–1043. https://doi.org/10.1016/j.petsci.2022.09.034.
Lookeren, J.V., 1983. Calculation methods for linear and radial steam flow in oil reservoirs. Soc. Petrol. Eng. J. 23 (3), 427–439. https://doi.org/10.2118/6788-PA.
Marx, J.W., Langenheim, R.H., 1959. Reservoir heating by hot fluid injection. SPE Trans 216 (1), 312–315. https://doi.org/10.2118/1266-G.
Miah, M.I., Elhaj, M.A., Ahmed, S., et al., 2018. Modeling of temperature distribution and oil displacement during thermal recovery in porous media: a critical review. Fuel 226, 423–440. https://doi.org/10.1016/j.fuel.2018.04.018.
Ni, X.F., Cheng, L.S., 2005. Calculating models for heating area of horizontal well bore in steam stimulation. Petrol. Explor. Dev. 32 (5), 108–112. https://doi.org/10.3321/j.issn:1000-0747.2005.05.025 (in Chinese).
Okoye, C.U., Tiab, D., 1982. Enhanced recovery of oil by alkaline steam flooding. In: SPE Annual Technical Conference and Exhibition. https://doi.org/10.2118/11076-MS.
Pang, Z.X., Lyu, X.C., Zhang, F.Y., et al., 2018. The macroscopic and microscopic analysis on the performance of steam foams during thermal recovery in heavy oil reservoirs. Fuel 233, 166–176. https://doi.org/10.1016/j.fuel.2018.06.048.
Pang, Z.X., Wang, L., Wu, Z.B., et al., 2019. An investigation into propagation behavior of the steam chamber during expanding-solvent SAGP (ES-SAGP). SPE J. 24 (2), 413–430. https://doi.org/10.2118/181331-PA.
Pang, Z.X., Wang, L., Yin, F.H., et al., 2021. Steam chamber expanding processes and bottom water invading characteristics during steam flooding in heavy oil reservoirs. Energy 234, 121214. https://doi.org/10.1016/j.energy.2021.121214.
Pang, Z.X., Wang, Q.H., Meng, Q., et al., 2024. The mechanisms of thermal solidification agent promoting steam diversion in heavy oil reservoirs. Pet. Sci. 21 (3), 1902–1914. https://doi.org/10.1016/j.petsci.2024.01.001.
Pawelec, A., Chmielewski, A.G., Licki, J., et al., 2016. Pilot plant for electron beam treatment of flue gases from heavy fuel oil fired boiler. Fuel Process. Technol. 145, 123–129. https://doi.org/10.1016/j.fuproc.2016.02.002.
Pratama, R.A., Babadagli, T.F., 2020. Effect of temperature, phase change, and chemical additives on wettability alteration during steam applications in sands and carbonates. SPE Reservoir Eval. Eng. 23 (1), 292–310. https://doi.org/10.2118/191188-PA.
Sandoval, M.M.I., Martínez, J.H.J., Muñoz, N.S.F., et al., 2023. Experimental investigation of EOR mechanisms for cyclic steam injection assisted by flue gas. Geoenergy Sci. Eng. 221, 211354. https://doi.org/10.1016/j.geoen.2022.211354.
Saripalli, H.K., Salari, H., Saeedi, M., et al., 2018. Analytical modelling of cyclic steam stimulation (CSS) process with a horizontal well configuration. Can. J. Chem. Eng. 96 (2), 573–589. https://doi.org/10.1002/cjce.22958.
Sasaki, K., Akibayashi, S., Kosukegawa, H., et al., 1996. Experimental study on initial stage of SAGD process using 2-dimensional scaled model for heavy oil recovery. In: SPE International Conference on Horizontal Well Technology. https://doi.org/10.2118/37089-MS.
Satar, V., Ozturk, H., 2024. Economic analysis of steam assisted underground mining of Bati Raman heavy oil field. Geoenergy Sci. Eng. 235, 212714. https://doi.org/10.1016/j.geoen.2024.212714.
Settari, A., Raisbeck, J.M., 1981. Analysis and numerical modeling of hydraulic fracturing during cyclic steam stimulation in oil sands. J. Petrol. Technol. 33 (11), 2201–2212. https://doi.org/10.2118/9078-PA.
Sharifipour, M., Nakhaee, A., Pourafshary, P., 2019. Model development of permeability impairment due to clay swelling in porous media using micromodels. J. Petrol. Sci. Eng. 175, 728–742. https://doi.org/10.1016/j.petrol.2018.12.082.
Shi, L.X., Ma, D., Li, X.L., et al., 2019. Analytical modeling of oil production rate during the entire steam-assisted gravity drainage process in heavy oil reservoirs. J. Petrol. Sci. Eng. 175, 190–199. https://doi.org/10.1016/j.petrol.2018.12.040.
Sun, F.R., Yao, Y.D., Li, X.F., et al., 2017. The mass and heat transfer characteristics of superheated steam coupled with non-condensing gases in perforated horizontal wellbores. J. Pet. Sci. Eng. 156, 460–467. https://doi.org/10.1016/j.petrol.2017.06.028.
Sylvester, N.B., Chen, H.L., 1988. An improved cyclic steam stimulation model for pressure-depleted reservoirs. In: SPE California Regional Meeting. https://doi.org/10.2118/17420-MS.
Tagavifar, M., Fortenberry, R., Rouffignac, E., et al., 2016. Heavy-oil recovery by combined hot water and alkali/cosolvent/polymer flooding. SPE J. 21 (1), 74–86. https://doi.org/10.2118/170161-PA.
Tamim, M., Ali, S.M.F., 1998. A new analytical cyclic steam stimulation model including formation fracturing. SPE J Can Pet Technol 37 (3). https://doi.org/10.2118/98-03-02.
Tao, L., Chen, Y., Liu, N.N., et al., 2022. A novel experimental method for the evaluation of residual oil distribution in a sand-packed model by using nitrogen and viscosity reducer huff-puff technology to develop heavy oil reservoirs. J. Petrol. Sci. Eng. 208, 109585. https://doi.org/10.1016/j.petrol.2021.109585.
Tewari, R.D., Abdalla, F., Lutfi, H.G., et al., 2011. Successful cyclic steam stimulation pilot in heavy oilfield of Sudan. In: SPE Enhanced Oil Recovery Conference. https://doi.org/10.2118/144638-MS.
Tiab, D., Okoye, C.U., Osman, M.M., 1982. Caustic steam flooding. J. Petrol. Technol. 34 (8), 1817–1827. https://doi.org/10.2118/9945-PA.
Wang, B., Huang, S.J., Zhao, F.L., et al., 2024. Investigating the heated zone evolution and production performance of cyclic steam stimulation with horizontal well in thick-layer heavy oil reservoirs. Geoenergy Sci. Eng. 241, 213108. https://doi.org/10.1016/j.geoen.2024.213108.
Wang, Z.J., Du, H.W., Li, S.Y., et al., 2023. Experimental study on gas-assisted cyclic steam stimulation under heavy-oil sandstone reservoir conditions: Effect of N_2/CO_2 ratio and foaming agent. Geoenergy Sci. Eng. 228, 211976. https://doi.org/10.1016/j.geoen.2023.211976.
Wu, Z.B., Liu, H.Q., Wang, X., 2018. 3D experimental investigation on enhanced oil recovery by flue gas coupled with steam in thick oil reservoirs. Energy Fuels 32 (1), 279–286. https://doi.org/10.1021/acs.energyfuels.7b03081.
Wu, Z., Vasantharajan, S., El-Mandouh, M., et al., 2009. Inflow performance of cyclic steam stimulation using horizontal well. In: SPE Kuwait International Petroleum Conference and Exhibition. https://doi.org/10.2118/127518-MS.
Yan, X.X., Pang, Z.X., Liu, D., et al., 2025. The characteristics of steam chamber expanding and the EOR mechanisms of tridimensional steam flooding (TSF) in thick heavy oil reservoirs. Geoenergy Sci. Eng. 244, 213434. https://doi.org/10.1016/j.geoen.2024.213434.
Zhang, N., Liu, W., Zou, X.F., et al., 2023a. Experimental study on thermochemical composite system huff-n-puff process in ultra-heavy oil production. Fuel 332, 126014. https://doi.org/10.1016/j.fuel.2022.126014.
Zhang, Q.C., Liu, H.Q., Kang, X.D., et al., 2021. An investigation of production performance by cyclic steam stimulation using horizontal well in heavy oil reservoirs. Energy 218, 119500. https://doi.org/10.1016/j.energy.2020.119500.
Zhang, Y., Li, B.F., Lu, T., et al., 2023b. Adaptation study on nitrogen foam flooding in thick reservoirs with high water cut and high permeability. Colloids Surf. A Physicochem. Eng. Asp. 657, 130539. https://doi.org/10.1016/j.colsurfa.2022.130539.
Zhu, W.Y., Li, B.B., Zhai, Y., et al., 2017. A new productivity prediction model for heavy oil reservoirs in the development pattern of steam huff and puff. Special Oil Gas Reservoirs 24 (3), 64–69. https://doi.org/10.3969/j.issn.1006-6535.2017.03.012 (in Chinese).